EXPERIMENTAL STUDY OF THE AXIAL FLOW THROUGH AN ANNULAR REGION WITH INNER CYLINDER ROTATION

Julio Manuel Barros Junior, jmb@puc-rio.br
Luis Fernando Alzuguir Azevedo, lfaa@puc-rio.br
Pontifícia Universidade Católica do Rio de Janeiro – PUC-RIO
Rua Marquês de São Vicente, 225 – Gávea, Rio de Janeiro - RJ

Abstract. *The flow between concentric cylinders with an inner rotating cylinder and with imposed pressure-driven axial flow was studied experimentally. The radius ratio was η = 0.64 and the aspect ration was Γ = 265. Friction factor and velocity fields were studied for four rotations of the inner cylinder and for laminar, transitional, and turbulent flow regimes. Velocity fields were measured by Particle Image Velocimetry (PIV). The results for friction factor showed that the influence of the rotation is more pronounced for the laminar and transitional flow regimes, increasing with the rotation of the inner cylinder. For these two flow regimes, increments of the order of 100% over the non-rotating case were observed.. The measured time-averaged axial velocity profiles presented a flat form with increasing inner cylinder rotation and axial Reynolds numbers. For turbulent flow, the influence of rotation in the velocity profiles was verified to be small.*

Keywords*: concentric annulus, rotating cylinder, pressure drop, axial flow, friction factor, piv.*

1. INTRODUCTION

The flow between concentric cylinders has been studied for the past years in great depth since Taylor's pioneering experiments and analysis (Taylor 1923). But very few works concentrated in measuring the velocity fields in a annular space for a wide range of Reynolds number.

Escudier and Gouldson (1995) studied the flow in a concentric annulus with axial pressure gradient for laminar, transitional and turbulent regimes. The axial and tangential velocity was measured with Laser Doppler Velocimetry. Also, the friction factor versus Reynolds number for a Newtonian and non-Newtonian fluid was obtained. In all cases the friction factor increased with the rotation of the inner cylinder. The influence of the rotation in the average axial velocity was more apparent for low Reynolds numbers.

Nouri and Withelaw (1997) made experiments in annular space for both concentric and eccentric cylinders, with rotation of the inner cylinder. The three velocity component was measured by Laser Doppler Velocimetry. Pressure drop of static pressure were also measured. The range of Reynolds numbers was from 8900 to 26600, which the increase of the friction factor was around 8% above the friction factor without rotation.

Wereley and Lueptow (1999) measured the instantaneous velocity fields using Particle Image Velocimetry (PIV) in an annular space with rotation of the inner cylinder and axial pressure gradient. The highest Reynolds number investigated was 25.

Loureiro (2004) investigated the flow in an annular space partially obstructed. Particle Image Velocimetry measured the velocity fields and was compared with numerical simulation.

The present work investigated experimentally the influence of the rotation of the inner cylinder in a concentric annular flow with axial pressure gradient. The main focus was to study a wide range of axial Reynolds number, with rotation speed of the inner cylinder close to the ones used in horizontal drilling process.

2. EXPERIMENTAL SET-UP

Figure 1 shows a schematic view of the test section. Two concentric pipes made the annular region. The inner cylinder was an aluminum pipe with 41.4mm of external diameter. The inner cylinder was divided into 4 pipes of 1.5 meters long each and they were carefully machined to assure there was no ovalization in the external diameter. To connect the 4 aluminum pipes, 3 special aluminum inner gloves was machined. The outer cylinder was composed of a 3 Pexiglas pipes with 2 meters long each and 64mm of inner diameter. Also, two special outer gloves was machined to attach the Pexiglas pipes with one an other, and as well to center the inner cylinder in the annular region, by means of three pins with 120º angle distance. Therefore, the length of the test section was 6 meters to assure flow development for both laminar and turbulent regimes. With these dimensions give a radius ration, η, of 0.64, and a length-to-hydraulic diameter ratio, Γ, of 265.

The flow through the test section was generated by gravity. To avoid pressure variation during the tests, a constant head on the superior tank was employed. This was accomplished by pumping the fluid from the inferior tank to the superior one and the excess fluid returned to the inferior tank through the return line pipe.

Two calibrated rotameters measured the flow rate. One rotameter, with 1000 l/h full scale, measured the low flow rates, including laminar and transitional flow regimes. The second rotameter, with 6000l/h full scale, measured the flow

rate for transitional and turbulent flow. To control the flow rate in the test section, a gate valve was assembled upstream to the inferior tank.

The inner cylinder was rotated by means of a 0.368kW WEG motor and pulley assembly attached to the end of the inner cylinder. The rotation speed was measured by an optical encoder formed by a slotted disk and a diode-photocell assembly.

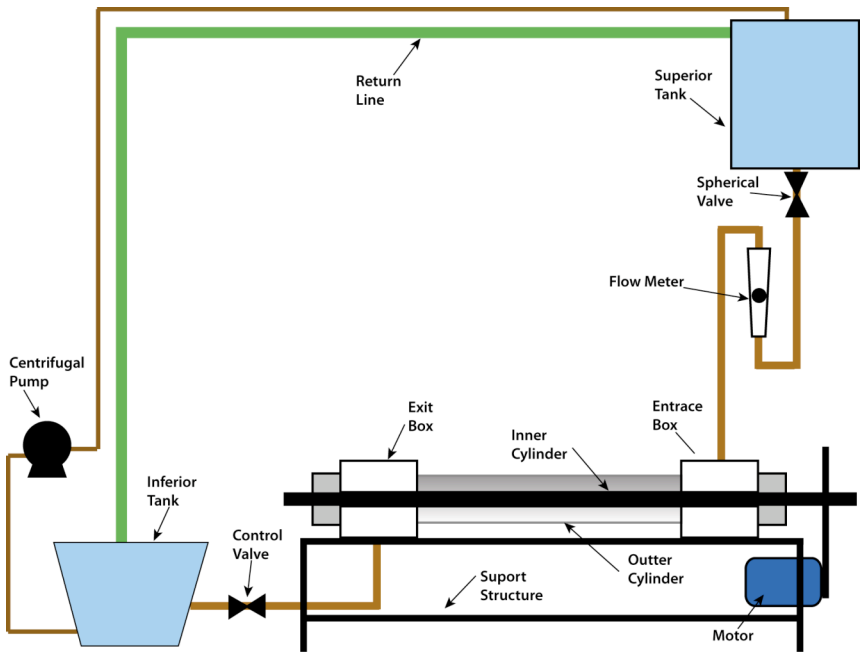

Figure 1. Schematic view of the test section.

Thirty three pressure taps were installed along the outside wall of the Plexiglas pipe. Each pressure tap consisted of a 2mm-diameter hole drilled in the Plexiglas tube, connected to a spherical valve, and to a 3mm diameter hose. The first pressure tap at the entrance of the pipe was used as a reference measurement and was connected to one leg of the manometer. The other 32 pressure taps were connected to hoses connected to a switching tank. The second leg of manometer was connected to the switching tank. Thereby providing means for selecting the desired position of the pressure tap to be measured. (Fig. 2). The space between each pressure taps in the first and second Plexiglas pipes was 200mm. In the third Plexiglas pipe the space was 150mm to increase the resolution of the measurements.

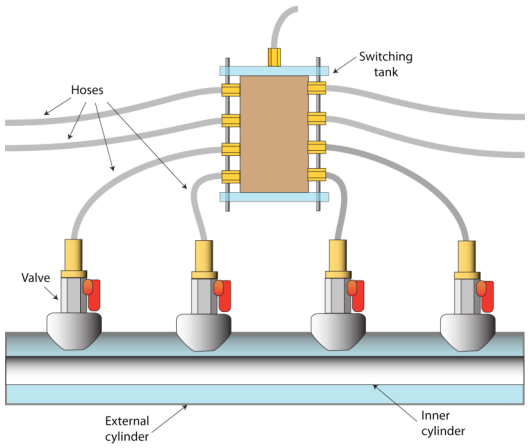

Figure 2. Schematic view of the pressure taps, hose, and the switching tank.

In order to measure the pressure drops with the required resolutions, a special manometer was designed and built. It consisted of an inverted “U” shape with two fluids (Fig. 3), one being the working fluid in the test section (water), and the second an oil with specific gravity of 0.815. With this manometer the readings of the pressure differences were amplified by a factor that inversely proportional to the difference of the specific gravity of the two fluids. This can be seen in the Eq. (1). In addition, the manometer designed could be inclined, amplifying even more the readings, if

necessary. In Eq. (1), h is the reading in the manometer (m); p_1 and p_2 are the pressures (Pa); ρ_1 is the density of the working fluid (kg/m^3); ρ_2 is the density of the manometer fluid (kg/m^3); sin α is the inclination angle of the manometer.

$$h = \frac{p_1 - p_2}{(\rho_1 - \rho_2) g \sin\alpha} \tag{1}$$

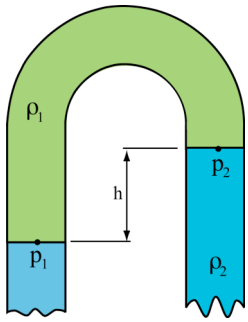

Figure 3. Schematic view of the inverted "U" shape manometer used.

The instantaneous and time-averaged velocity field in the annular region was measured using a two-component Particle Image Velocimetry system. Figure 4 shows a schematic view of the setup for the PIV system used. As shown in Fig. 4, the laser was mounted in an optical table that provided flexibility in positioning the laser. This optical table was assembled to an aluminum base structure (Bosch Inc.), which also provided flexibility in positioning the camera. Special care was taken to positioned the laser in the meridional plane section of the annular space, to avoid anomalous apparent radial velocity components caused by the azimuthal path of the particles through the thickness of the laser light sheet. A visualization box was assembled at 215 hydraulic diameters from the entrance of the test section, where the data were taken by the PIV technique. This box minimizes the optical distortions due to the curvature of the the Plexiglas pipe when filled with the working fluid.

The system consisted of a TSI 4 Megapixel, 12 bits camera, synchronized to a double cavity New Wave Pegasus Nd:YAG laser, with an energy of 120mJ/pulse. The laser light sheet was formed by one -15-mm cylindrical and a 500-mm spherical lenses. A 105-mm micro Nikkor lens was attached to the camera. Hollow glass spheres with metal coating (Potters Inc), with average diameter of 13µm were used as seed particles. The images pairs were capture and processed in Insight 3G software (TSI Inc.). A multigrid, integer windows shift, and a second order correlation (Hart, 1998) were used to process the images. The final grid was 64x64 pixels with 50% window overlap.

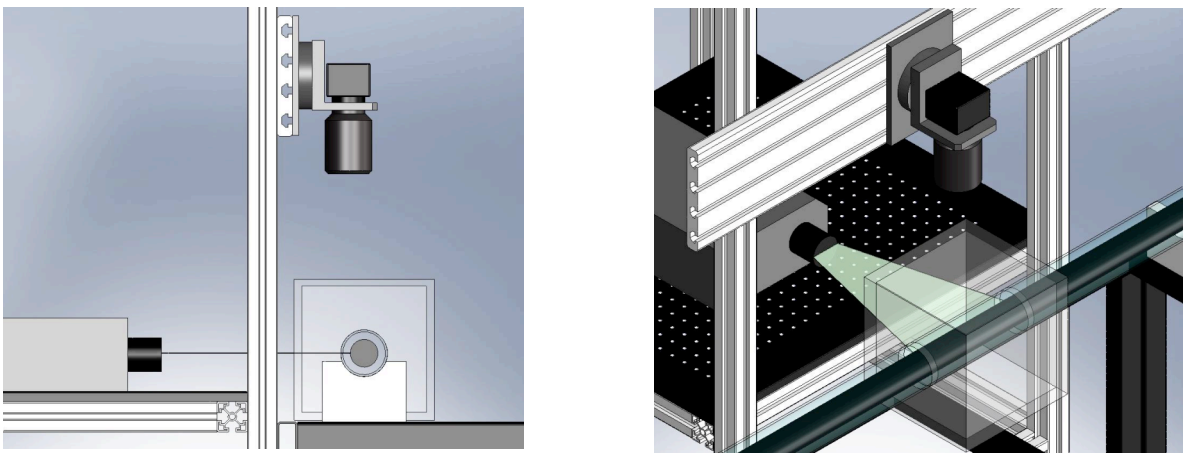

Figure 4. Schematic views of the PIV system.

3. RESULTS

This section presents the results for pressure drop and the axial velocity profiles. The pressure drop results are presented in the form of friction factors as a function of the axial and rotational Reynolds numbers. The velocity profiles, obtained with the PIV technique, reveal the influence of the inner cylinder rotation o the flow characteristics.

A total of 95 experiments were conduct, 50 for pressure drop and 45 for velocity field measurements. The range of the axial Reynolds investigated ranged from 225 to 8456, for 4 different values of the rotational Reynolds numbers, namely, 0, 300, 500, 900.

The axial Reynolds number was calculated by the Eq. 2, where ρ is the density of the working fluid (kg/m^3), Q is the volumetric flow rate (m^3/s), A is the cross sectional area of the annular region (m^2), and μ is the viscosity of the working fluid (Pa.s). D_H is the hydraulic diameter (m) given by $D_H = 4A/Pm$.

$$\mathrm{Re}_{axial} = \frac{\rho Q D_H}{A\mu} \tag{2}$$

The rotational Reynolds number was calculated by the Eq. 3, where Ω is the rotational speed of the inner cylinder (rad/s), r_i is the inner cylinder radius (m), and d is the annular spacing (m).

$$\mathrm{Re}_{rot} = \frac{\rho \Omega r_i d}{\mu} \tag{3}$$

The developed region of the annular section was determined by ploting the pressure data *versus* distance, like the one that is presented in Fig. 5. To obtain the pressure gradient (ΔP/L), a linear least square fit method was applied in the developed region of the annular space. The angular coefficient of the linear equation represents the pressure gradient, used to obtain the friction factor.

The friction factor was evaluated by using Eq. 4, where ΔP/L is the pressure gradient (Pa/m) along the annular region.

$$f = \frac{2(\Delta P / L) D_H}{\rho (Q/A)^2} \tag{4}$$

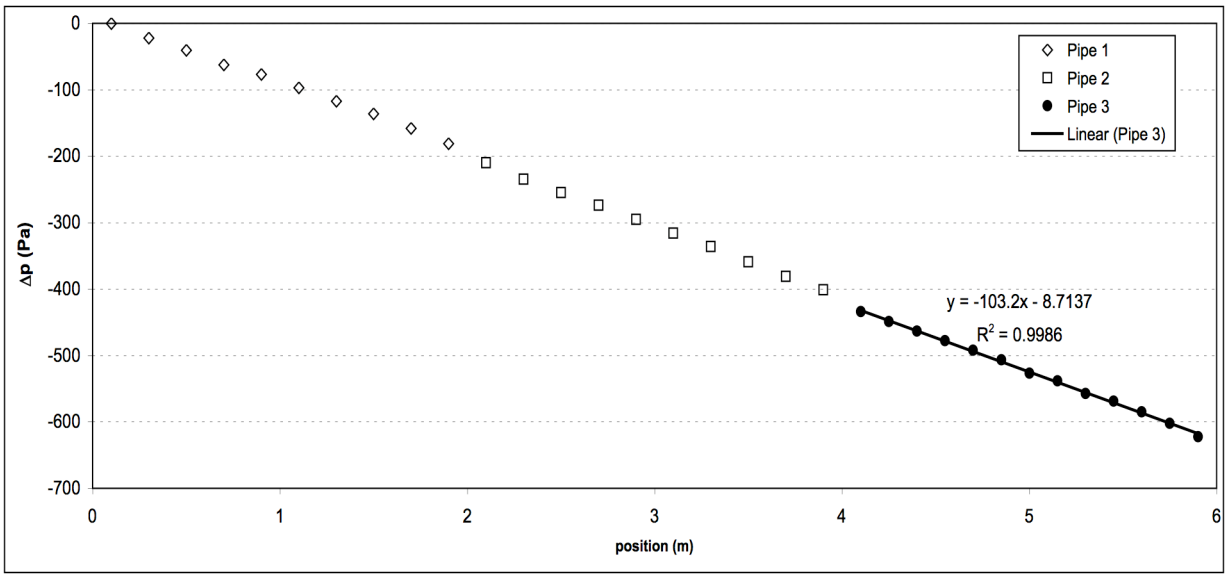

Figure 5. Pressure versus distance plot for Re_{axial} = 8456 without inner cylinder rotation.

3.1. Friction Factor Results

The effect of the rotation of the inner cylinder on the friction factor is shown in Fig. 6. In the figure the solid line represents the analytical solution of the *f versus* Re dependence for flow through an annulus for the laminar regime, as proposed by White (1978). The dashed line is the turbulent dependence for *f versus* Re proposed by Miller and found, for instance, in Fox & McDonald (1998). In this correlation, the hydraulic diameter is used. These lines serve as base cases for comparison purposes. The symbols in the figures are cued to the rotational Reynolds numbers indicated in the figure.

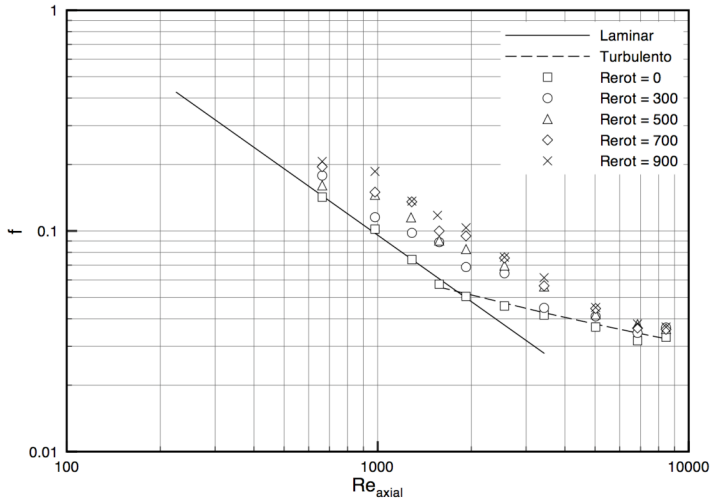

Figure 6. Effect of the inner cylinder rotation on the friction factor.

An observation of the figure shows clearly that the friction factor is heavily influenced by the rotation of the inner cylinder for axial Reynolds numbers especially in the laminar and transitional regimes. As the Reynolds number increases to the turbulent regime, the influence of the rotation is decreased, but still relevant.

A better assessment of the influence of rotational Reynolds in the friction factor can be obtained with the help of Fig. 7. This figure presents the ratio of the friction factor with rotation by the friction factor without rotation, f/f_0, for all the axial and rotational Reynolds numbers investigated. For the highest value of rotational Reynolds investigated, Re_{rot}=900, the increase in the friction factor varies from 100% for Re_{axial} = 1576 to 10% for Re_{axial} = 8456. The same trend is observed for all values of the rotational Reynolds number indicating that as the Reynolds increase to the turbulent regime the effect of rotation loses importance.

Indeed, the decrease in f/f_0 from 100% to 10% is observed for all values of rotational Reynolds investigated.

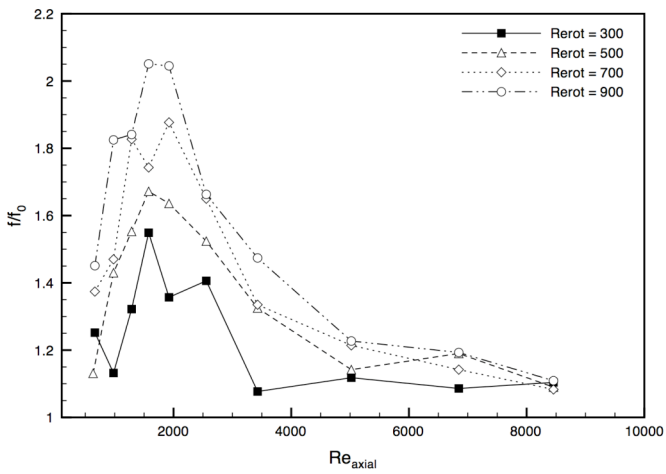

Figure 7. Effect of the rotation on the ratio of the friction factor, f/f_0.

3.2. Velocity Profile Results

The axial velocity profiles to be presented here were obtained from the PIV technique by averaging over 150 instantaneous velocity fields. From these averaged velocity fields, radial profiles of axial velocity were extracted. It should be mentioned that time-averaged velocity profiles extracted from different axial positions along the annular region displayed remarkable coincidence. Also, the velocity fields were taken approximately 215 hidraulic diameters from the entrance of the test section.

Figure 8 and Fig. 9 show the averaged axial velocity profiles. In these figures the y-axis is the dimensionless axial velocity while the x-axis represents the dimensionless radial coordinate, where y/δ=0 corresponds to the outer wall and y/δ=2 corresponds to the inner rotating wall. Each figure displays the velocity profiles for three values of the rotational Reynolds number, namely, 0, 300 and 900.

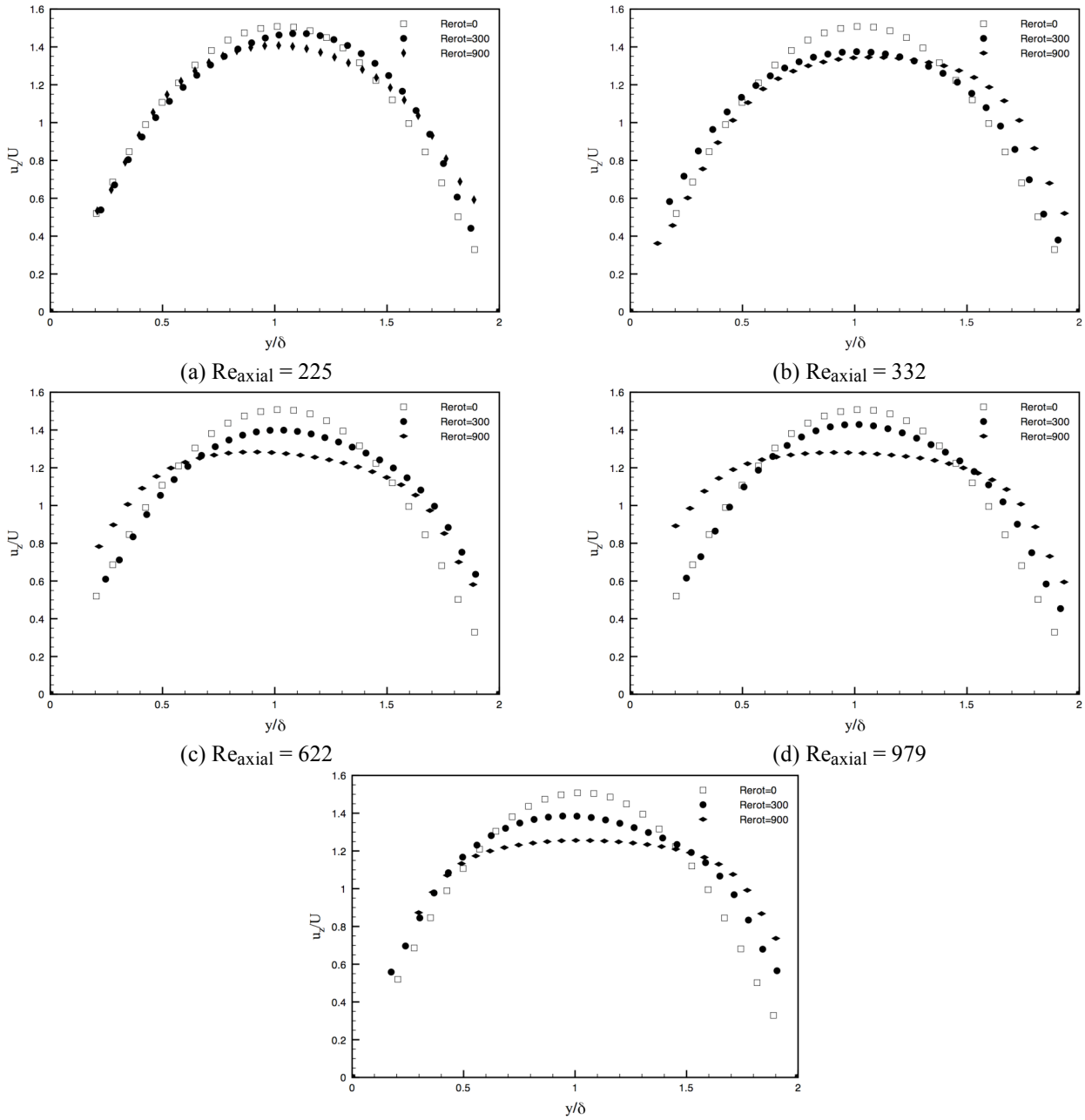

(a) Re_{axial} = 225

(b) Re_{axial} = 332

(c) Re_{axial} = 622

(d) Re_{axial} = 979

(e) Re_{axial} = 1287

Figure 8. Effect of the rotation inner cylinder on the axial velocity profiles from Re_{axial} = 225 to 1287.

It can be seen in Fig. 8(a) for Re_{axial} = 225, that the characteristic parabolic profile of laminar flow through an annular region without rotation is gradually flattened and distorted as the rotation increases. This change in the shape of the profile can be attributed to the transfer of the axial momentum promoted due to the presence of the secondary motion associated with the rotation of the inner cylinder. As the rotational Reynolds number increases, the velocity profile becomes flat, losing the characteristic parabolic shape. A comparison of the velocity profiles of the Fig. 8(b) and Fig. 8(c) indicates that for the higher values of the axial Reynolds number the velocity profile becomes more resistant to deformation, demanding a higher value of the rotation Reynolds number to deform. This observation is even more evident if one compares Fig 8(d) and Fig. 8(e), in which the axial Reynolds number is higher, although still in the laminar regime.

In the cases of Fig 9(a) to Fig. 9(d) the shape of the velocity profiles is totally altered as a consequence of the establishment of turbulent flow regime. Not only the shape of the profiles becomes flatter, as expected for this regime, but also the influence of the rotation of the inner cylinder becomes less significant. Indeed, a small difference between the velocity profiles can be observed in Fig. 9(a), for Re_{axial} = 3428, for the three Re_{rot} values. This small difference

progressively vanishes as the axial Reynolds number increases. In Fig. 9(d) for Re_{axial} = 8456 the velocity profiles can be considered coincident.

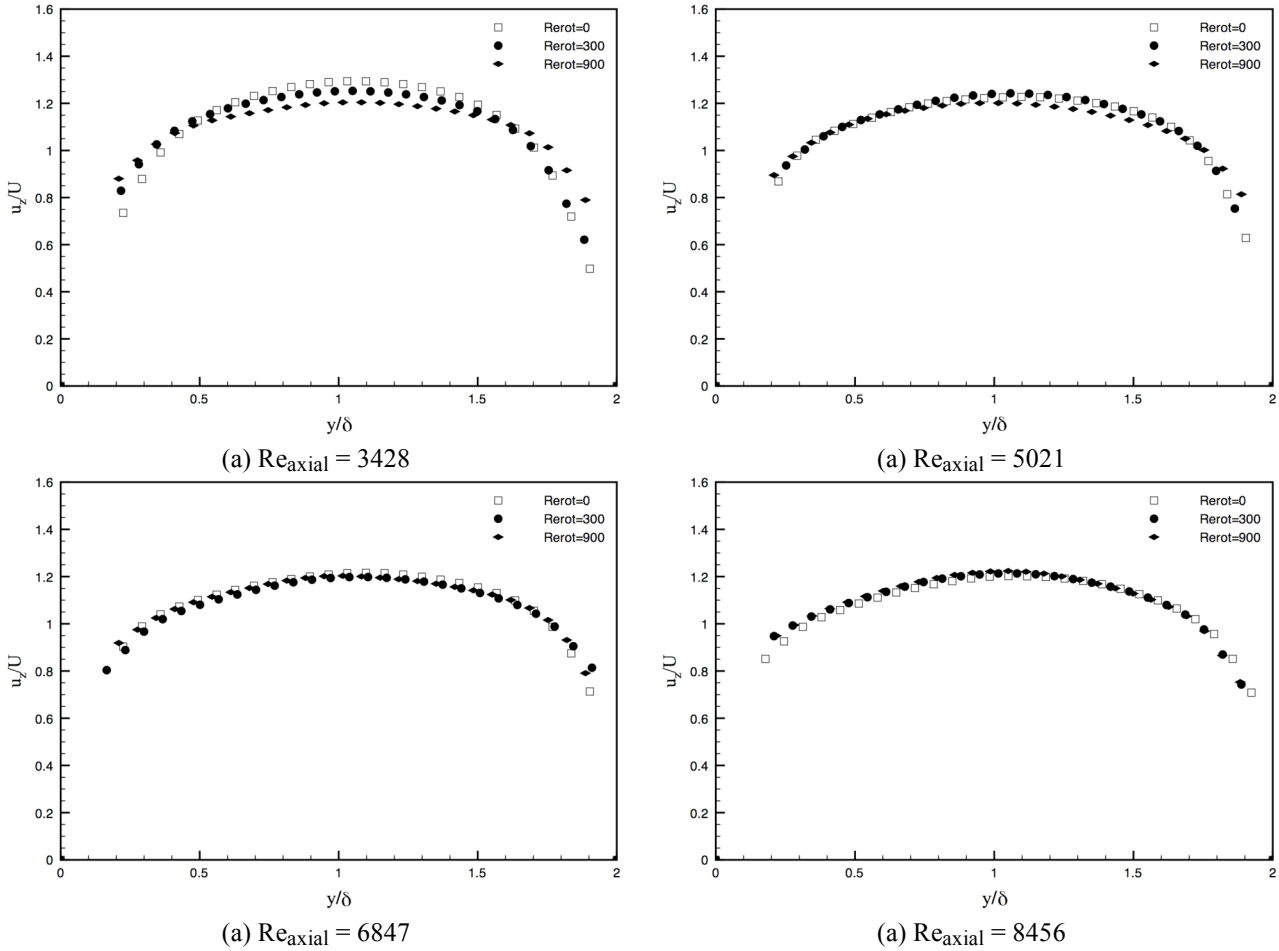

(a) Re_{axial} = 3428 (a) Re_{axial} = 5021

(a) Re_{axial} = 6847 (a) Re_{axial} = 8456

Figure 9. Effect of the rotation inner cylider on the axial velocity profiles from Re_{axial} = 3428 to 8456.

3.3 Comparison between Velocity Profile and Friction Factor

The behavior just presented for the axial velocity profiles can help to understand the effects of the rotation of the inner cylinder previously the friction factor shown in section 3.1. As mentioned before, the effect of the rotation on the friction factor is more significant for small axial Reynolds numbers, becoming maximum for Reynolds near the transitional flow regimes, and decaying as the Reynolds number increases. This behavior of the friction factor can be linked to the changes in the velocity profiles presented.

Although velocity data very close to the wall could not be obtained to due image distortions in these regions, a close observation of the velocity profiles, presented in Fig. 8(a) and Fig 8(e), shows an increase of the velocity gradient close to the wall, if compared to the velocity profile without rotation. For the case of Re_{axial} = 225 and Re_{axial} = 332 (Fig. 8(a) and Fig. 8(b)), the increase of the velocity gradient is more apparent close to the inner rotation wall (y/δ=2). For Re_{axial} = 622 and 980 (Fig. 8(c) and Fig. 8(d)) the increase is noted on both walls, justifying the higher friction factor For the cases in which the turbulent regimes prevails (Fig. 9), only small differences can be noticed in the velocity gradient close to the wall. This fact justifies the small variation on the friction factor for these axial Reynolds numbers.

4.CONCLUSIONS

The present paper presents an experimental investigation on the influence of inner cylinder rotation on the friction factor and characteristics of axial flow through an annular region.

Pressure drop data revealed that rotation of the inner cylinder could significantly alter the pressure drop through the annular region for the laminar and transition flow regimes. In the turbulent regime, rotation of the inner cylinder has a relatively weaker effect.

5. REFERENCES

Barros Jr, J.M., 2007, "Estudo Experimental do Escoamento Axial através de Região Anular com Rotação do Cilindro Interno", Master's Thesis, Pontifícia Universidade Católica do Rio de Janeiro.

Escudier, M.P., Gouldson, I.W., 1995, "Concentric Annular flow With Centerbody Rotation of a Newtonian and a Shear-Thinning Liquid", International Journal Of Heat And Fluid Flow, 16(3):156–162.

Foucaut, J.M., Miliat, B., Perenne, N., Stanislas, M., 2004, "Characterization of Different PIV Algorithms Using the Europiv SIG and Real Images from a Turbulent Boundary Layer", Proceedings of The Europiv.

Hart, D.P., 1998, "The Elimination of Correlation Errors in PIV Processing", International Symposium on Applications of Laser Techniques To Fluid Mechanics.

Loureiro, B.V., 2004, "Escoamento Secundário em um Anular Parcialmente Obstruído com Rotação do Cilindro Interno" Phd Thesis, Pontifícia Universidade Católica do Rio De Janeiro.

Nouri, J.M., Whitelaw, J.H., 1997, "Flow of newtonian and non-newtonian fluids in an eccentric annulus woth rotation of the inner cylinder", Internation Journal of Heat and Fluid Flow, 18:236-246.

Rabello, P.C., Alves, D.P., Barros Jr, J.M., Loureiro, B.V., Azevedo, L.F.A., 2004, "Medição Do Escoamento Axial Em Um Espaço Com Rotação Do Cilindro Interno", Congresso de Estudantes de Engenharia Mecânica.

Raffel, M., Willert, C., Kompenhans, J., 1998, "Particle Image Velocimetry: A Practical Guide" Springer.

Tavara, D.I.M., 2005, "Queda De Pressão em Escoamento Axial através de Região Anular com Rotação do Cilindro Interno", Master's Thesis, Pontifícia Universidade Católica do Rio De Janeiro.

Taylor, G.I., 1923, "Stability of s Viscous Liquid Contained Between Two Rotating Cylinders".

Wereley, S.T., Lueptow, R.M., 1999, "Velocity field For Taylor-Couette flow With An Axial flow", Physics Of Fluids, 11(12).

Westerweel, J., 1997, "Fundamentals Of Digital Particle Image Velocimetry", Measurements and Science.

6. RESPONSIBILITY NOTICE

The author(s) is (are) the only responsible for the printed material included in this paper.